A unified spectral parameterization for wave breaking: From the deep ocean to the surf zone

J.-F. Filipot[1] and F. Ardhuin[2]

Received 29 November 2011; revised 16 February 2012; accepted 8 March 2012; published 24 April 2012.

[1] A new wave-breaking dissipation parameterization designed for phase-averaged spectral wave models is presented. It combines wave breaking basic physical quantities, namely, the breaking probability and the dissipation rate per unit area. The energy lost by waves is first explicitly calculated in physical space before being distributed over the relevant spectral components. The transition from deep to shallow water is made possible by using a dissipation rate per unit area of breaking waves that varies with the wave height, wavelength and water depth. This parameterization is implemented in the WAVEWATCH III modeling framework, which is applied to a wide range of conditions and scales, from the global ocean to the beach scale. Wave height, peak and mean periods, and spectral data are validated using in situ and remote sensing data. Model errors are comparable to those of other specialized deep or shallow water parameterizations. This work shows that it is possible to have a seamless parameterization from the deep ocean to the surf zone.

Citation: Filipot, J.-F., and F. Ardhuin (2012), A unified spectral parameterization for wave breaking: From the deep ocean to the surf zone, *J. Geophys. Res.*, *117*, C00J08, doi:10.1029/2011JC007784.

1. Introduction

[2] The understanding of wave breaking in the physical space is far from complete [e.g., *Banner and Peirson*, 2007; *Babanin*, 2009]. Accordingly, defining its spectral signature, used in numerical wave models, is a great challenge. This is precisely the issue addressed in this paper. With a discretization of the surface elevation spectrum E over frequencies f and directions θ, the spectral models used for wave forecasting and hindcasting solve the wave energy balance equation [*Gelci et al.*, 1957]

$$\frac{\mathrm{d}E(f,\theta)}{\mathrm{d}t} = S_{atm}(f,\theta) + S_{nl}(f,\theta) + S_{oc}(f,\theta) + S_{bot}(f,\theta). \quad (1)$$

Following a wave packet in physical and spectral space, the spectral wave energy density, E, evolves due to an atmospheric source S_{atm}, the energy exchanges between spectral components S_{nl}, an ocean source S_{oc} and a bottom source S_{bot} [see *WISE Group*, 2007; *Ardhuin et al.*, 2010]. This decomposition is rather arbitrary as, for instance, the breaking dissipation involved in S_{oc} is tightly related to the nonlinear processes represented in S_{nl}. Yet, it allows the determination of energy and momentum sources, useful for coupling waves with the atmosphere and oceans [e.g., *Janssen et al.*, 2004].

[3] Here we define the ocean source S_{oc} as the sum of two distinct terms

$$S_{oc}(f,\theta) = S_{bk}(f,\theta) + S_{cu}(f,\theta), \quad (2)$$

where S_{bk} is the spontaneous dissipation that occurs when waves become too steep and break, and S_{cu} is a "cumulative" induced by large-scale breakers overtaking short waves, as observed by *Banner et al.* [1989].

[4] The source function S_{bk} has been extensively discussed in the literature. Because it is generally used as a tuning term without any quantitative link to measurable wave properties [*WISE Group*, 2007; *Ardhuin et al.*, 2010], a wide variety of plausible expressions have been proposed for its parameterization. Building on the ideas of *Phillips* [1984] and the observations of *Banner et al.* [2000] and *Ardhuin et al.* [2009, 2010] produced a deep water breaking parameterization that is consistent with these breaking observations, and gives more accurate results than previous empirical parameterizations [e.g., *WAMDI Group*, 1988; *Bidlot et al.*, 2005; *Tolman et al.*, 2011]. However, that work still uses a direct parameterization of the wave breaking from the wave spectrum. In particular, the dissipation rate for waves of a given frequency is a function of the spectral density at that frequency only. Clearly, as pointed out by *Phillips* [1984], this can only be realistic for a slowly varying spectral density. In general, the dissipation should be a function of the frequency bandwidth over which the wave energy is distributed. For example, a monochromatic wave train of very small amplitude has no breaking wave but a very large spectral density, and a parameterization from the local spectral saturation would predict some breaking-induced dissipation.

[1]Service Hydrographique et Océanographique de la Marine, Brest, France.
[2]Laboratoire d'Océanographie Spatiale, Ifremer, Plouzane, France.

0148-0227/12/2011JC007784

Table 1. Effects of Depth Limitation on Wave Growth, According to Different Parameterizations[a]

Model Parameterizations	H_s for h = 1000 m (m)	H_s for h = 15 m (m)
Bidlot et al. [2005] and DB0	7.6	8.3
Bidlot et al. [2005] and BJ78	7.6	4.9
TEST441b [*Ardhuin et al.*, 2010] and BJ78	7.3	5.3
TEST500 (this paper) and DB0	8.3	3.5
Empirical	9	2.3

[a]These numbers were obtained by running the WAVEWATCH III model over a rectangular Cartesian grid of constant water depth h, covering 300 km in the downwind direction and 100 km in the cross-wind direction, and blowing a constant 20 m s^{-1} wind. DB0 means that there is no specific parameterization for depth-induced breaking, and BJ78 refers to *Battjes and Janssen* [1978]. The empirical parameterization is taken from *Young and Verhagen* [1996]. Given the possible variability of bottom friction, the calculations were performed here without bottom friction.

[5] Beyond the necessities of spectral wave modeling, many applications would benefit from an explicit estimation of breaking wave properties. For example, the height of breaking waves is needed for upper ocean mixing [e.g., *Agrawal et al.*, 1992; *Rascle and Ardhuin*, 2009]. *Banner and Morison* [2010] are among the first to provide the dominant breaking crest length density as an output of their wave model.

[6] Two major causes may explain the lack of appropriate spectral wave-breaking formulation: the insufficient understanding of the underlying physical processes, and the difficulty to reflect the strongly nonlinear physical features of the breaking process in the linear spectral framework of the wave forecasting models. From a theoretical point of view, the wave-breaking-induced dissipation rate per unit area may be decomposed in the product of (1) a breaking probability Q, (2) a crest length density per unit area Π, and (3) a dissipation rate per unit length of breaking crest ϵ. Therefore, to obtain a proper parameterization of S_{bk}, it is desirable to parameterize these quantities explicitly, under a form suitable to the framework of spectral models.

[7] *Filipot et al.* [2010, hereinafter FAB] proposed a parameterization of the breaking probability derived from the wave spectrum. In that work, waves are decomposed in scales with overlapping spectral contents. This concept of scale is a combination of the usual spectral component but with particular finite spectral bandwidth that is proportional to the central frequency, which provides a meaningful amplitude of the signal. The price of this decomposition is its nonorthogonal nature, such that a given wave frequency is included in several wave scales. A positive aspect is that, for the dominant waves, this analysis is consistent with the work of *Banner et al.* [2000], and provides a method for extending it to shorter or longer-wave components. The FAB formulation relies on the observation that, whatever the water depth, waves break when their crest orbital velocities u_c approaches their phase velocity C [e.g., *Wu and Nepf*, 2002; *Stansell and MacFarlane*, 2002]. This allows the breaking probability parameterization P_{FAB} to be operative from deep to shallow water. In the present study, following FAB, we use this breaking criterion, $u_c/C \simeq 1$, in a single wave-breaking source term S_{bk}, which we expect to be valid from the deep ocean to the surf zone.

[8] This parameterization is obtained by combining the breaking probability per wave scale proposed by FAB, with an estimation of the dissipation rate in each breaker. This gives the source function S_{bk}. The rest of the physical parameterizations, air-sea interaction and cumulative breaking, is described by *Ardhuin et al.* [2010] and will be shortly summarized in section 6. For a better understanding of the present work, the reader is invited to consult these papers.

[9] In our approach, the dissipation rate of wave energy will be first assessed in the physical space for each wave scale by combining parameterizations of Q, ϵ and Π. This dissipation is finally distributed over the appropriate spectral components, yielding S_{bk}. Because the parameterizations of Q, ϵ and Π are designed to be applicable in all water depths, the new source terms should also apply everywhere. So far, two distinct terms represent the breaking-induced dissipation, one for the deep water (whitecapping), another for the depth-induced breaking [e.g., *WISE Group*, 2007]. Such a combination generally provides too weak dissipation in finite depth conditions over a flat bottom. There, the traditional whitecapping parameterizations do not fully take into account the wave steepening and stronger dissipation rates, and the water is too deep for the so-called "depth-induced breaking" term to be very effective, as illustrated in Table 1. The existing parameterizations overpredicted the expected wave heights for depth-limited growth by a factor of 2 or more.

[10] As far as we know, the present study is the first attempt to build a single parameterization able to model this transition. Although the parameterization proposed here is not the final answer, it is a step in this direction.

2. Concepts of the New Source Term

[11] Because we need to relate spectral and wave by wave analysis, we use the wave scales defined by FAB. Each wave scale is centered on a frequency f_i, and has a finite spectral bandwidth covering the range from $f_{i,-} = 0.7f_i$ to $f_{i,+} = 1.3f_i$, similar to the range used by *Banner et al.* [2000] for dominant waves. In practice the wave scale selection can be achieved by filtering the spectrum with an appropriate window. For their purpose, FAB used a Hann window to prevent spectral leakage, here we shall prefer a rectangular window, which should not affect the results and simplify the calculation. Sliding the window along the frequency axis gives a range of scales f_i, as illustrated by Figure 1. In practice, i varies from 1 to N, with N such that $f_{N,+}$ corresponds to the last frequency in the model. The number of wave scales, N is thus slightly less than the amount of frequencies defined in the model. A representative wave height H_r and wave number $\bar{k}_r$ for each wave scale f_i are defined by

$$H_r(f_i) = \frac{4}{\sqrt{2}}\sqrt{\int_0^\infty W_i(f)E(f)df}, \tag{3}$$

$$\bar{k}_r(f_i) = \frac{\int_0^\infty W_i(f)k(f)E(f)df}{\int_0^\infty W_i(f)E(f)df}, \tag{4}$$

where the filtering window is defined by $W_i(f) = 1$ for $f_{i,-} < F < f_{i,+}$ and $W_i(f) = 0$ otherwise. From the two

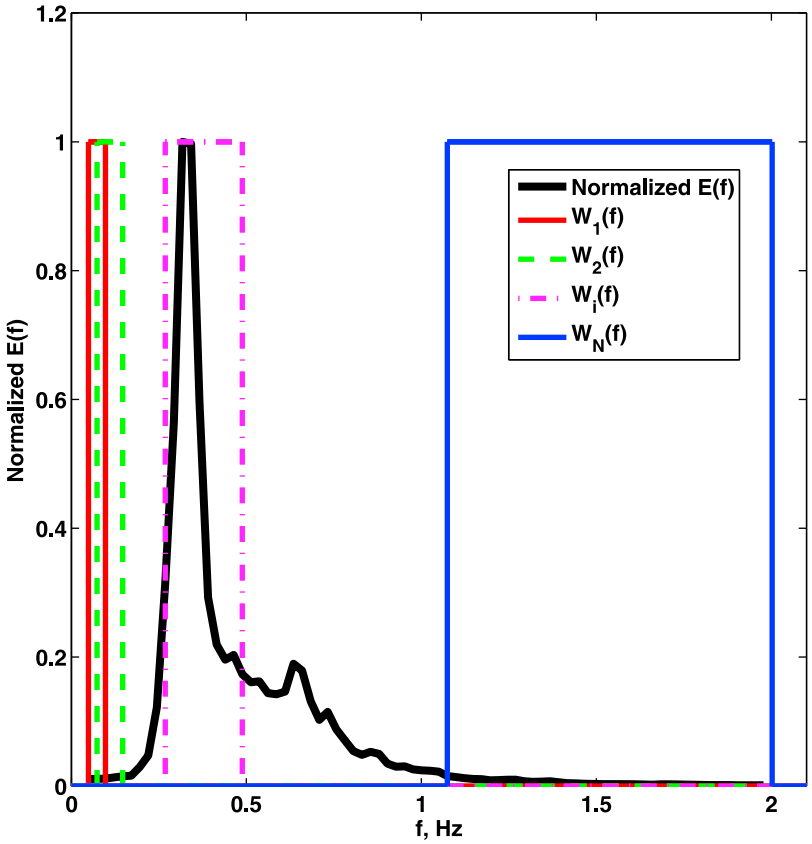

Figure 1. Illustration of the wave scale selection. The black line is a normalized frequency wave spectrum. The colored lines show the filtering windows $W_i(f)$. Only a few windows are shown for sake of clarity. In the general case, the $W_i(f)$ is 1 between $f_{i,-} = 0.7f_i$ and $f_{i,+} = 1.3f_i$ and zero elsewhere. From the energy bandwidth selected by this process, some characteristic properties of the wave scales can be derived, following equations (2) and (4).

quantities $H_r(f_i)$ and $\bar{k}_r(f_i)$ we shall define the parameterizations of $Q(f_i)$, $\epsilon(f_i)$, $\Pi(f_i)$. The dissipation rate per unit area for each scale reads

$$D(f_i) = Q(f_i) \times \epsilon(f_i) \times \Pi(f_i). \tag{5}$$

The last step consists in attributing $D(f_i)$ to the spectral components that contribute to the scale f_i, i.e., those with frequencies in the scale bandwidth. This attribution is achieved by weighting $D(f_i)$ proportional to the wave spectral density. Thus, for a given wave scale f_i, the most dissipated components are the most energetic

$$S_{bk,i}(f) = \frac{D(f_i) \times E(f)}{\int_0^\infty E(f) W_i(f) df}. \tag{6}$$

Finally, because each spectral component f is associated with several wave scales, from f_j to f_k, the final source term $S_{bk}(f)$ is given as follows:

$$S_{bk}(f) = \frac{1}{k-j+1} \sum_{i=j}^{k} S_{bk,i}(f). \tag{7}$$

For further informations on the model and its implementation, the interested reader may refer to Appendix A. The parameterizations of the needed quantities Q, ϵ and Π will be presented and discussed in the following sections.

[12] One of the weaknesses of the present approach is that it does not distinguish between different directional wave distributions, as everything is parameterized from the frequency spectrum only.

3. Parameterization of the Breaker Height Distribution

[13] Because we use a dissipation rate per unit crest length that depends on wave heights, as presented in section 4, we need a parameterization of the breaker height distribution [e.g., *Thornton and Guza*, 1983] instead of the breaking probability. We use here the breaker height distribution parameterized by FAB. This work was based on *Miche* [1944] who demonstrated that, for regular waves, the breaking criterion $u_c/C = 1$ can be expressed as $kH/\tanh(kh) \simeq \beta_t$, with k the wave number, H the wave height, h the water depth and $\beta_t = 0.88$ a breaking threshold. The expression proposed by FAB relies on the product of the Rayleigh distribution P_R times a breaking weight W_B, both estimated for each wave scale f_i. The function W_B is mainly based on Miche's work and enables to pass from the distribution of all wave heights to the distribution of

the broken wave heights only, $P_B = P_R \times W_B$. P_B is the breaker height distribution per wave scale with

$$P_R(H, f_i) = \frac{2H}{H_r^2(f_i)} \exp\left(-\left(\frac{H}{H_r(f_i)}\right)^2\right), \quad (8)$$

$$W_B(H, f_i) = 1.5\left[\frac{\beta_r}{\beta_{t,\mathrm{lin}}}\right]^2 \left\{1 - \exp\left[-\left(\frac{\beta}{\beta_{t,\mathrm{lin}}}\right)^4\right]\right\}, \quad (9)$$

where $\beta_r = \bar{k}_r(f_i)H_r(f_i)/\tanh(\bar{k}_r(f_i)h)$, $\beta = \bar{k}_r(f_i)H/\tanh(\bar{k}_r(f_i)h)$ and $\beta_{t,\mathrm{lin}}$ is a breaking threshold, as defined by *Miche* [1944] but taking the linearization of the waves into account. We note that the breaking probability for the wave scale f_i is

$$Q_B(f_i) = \int_0^\infty P_B(H, f_i)dH. \quad (10)$$

This parameterization was calibrated over intermediate water conditions and further validated in deep and shallow water [*Filipot et al.*, 2010].

4. The Crest Length Density Per Unit Area, Π

[14] The variable $\Pi(f_i)$ is the crest length density per unit area for waves with scale f_i. Each wave scale f_i comprises wave numbers ranging from $0.49k(f_i)$ to $1.69k(f_i)$ in deep water (with $k(f_i)$ the wave number corresponding to f_i from the linear theory). We use the crest length density for monochromatic unidirectional waves as an approximation

$$\Pi(f) = \frac{k(f)}{2\pi}. \quad (11)$$

[15] This assumption is likely appropriate for the dominant waves, which have a low directional spread. Now the spectral density of the crest length spatial density is taken to be

$$\Pi^*(f) = \frac{k(f)}{2\pi\Delta k(f)}. \quad (12)$$

In deep water, $\Pi^*(f) \simeq 0.13$ which is indeed consistent with in situ measurements by *Scott et al.* [2005] that give $\Pi^*(f)$ in the range 0.1–0.2. As shallow water waves have a narrower directional distribution we expect equation (11) to be applicable in shallow water as well.

5. Dissipation Rate Parameterization

[16] Two major theories exist for assessing the energy loss associated with breaking: the roller model [*Duncan*, 1981, 1983] and the bore model [e.g., *Thornton and Guza*, 1983; *Chawla and Kirby*, 2002]. These two approaches share nonetheless a common feature as they both rely on the study of steady breakers.

5.1. The Roller Model

[17] The roller model provides the dissipation rate from the tangential stresses acting at the interface between the zone of turbulent water (the roller) and the undisturbed flow [*Longuet-Higgins and Turner*, 1974].The roller is here assumed to be stationary, an hypothesis validated by the observations of *Cointe and Tulin* [1994]. *Duncan* [1981] conducted extensive tank experiments with "deep water" wave breaking over a submerged hydrofoil, in order to relate the dissipation inferred from the roller theory to the momentum deficit due to breaking in the turbulent wake following a steady breaker. He first showed that the roller weight was balanced by Reynolds stresses acting at the interface

$$\bar{\tau}L = \bar{\rho}'gA, \quad (13)$$

with g the gravity acceleration, $\bar{\tau}$ the Reynolds shear stress, and $\bar{\rho}'$ the aerated region density, both averaged over the breaker length L. As this stress is associated with the momentum deficit in the breaker wake, Duncan found the following expression for the energy dissipated by breaking per unit crest length:

$$\epsilon_{Du} = \rho_w \frac{bC^5}{g}, \quad (14)$$

with $b = 0.045$, g the gravity and ρ_w the water density. Also in deep water, but relaxing the stationarity assumption, *Melville* [1994] gave an alternative estimation of the dissipation rate. Based on laboratory observations of *Rapp and Melville* [1990], he found the same form of the dissipation rate as Duncan (equation (14)), but reported that b may vary from 3.2×10^{-3} to 1.6×10^{-2}. In a recent study and from measurements of the energy lost by 2D breakers in a wave tank, *Banner and Peirson* [2007] estimated $b \simeq 8 \times 10^{-5} - 1.2 \times 10^{-3}$. This wide range of values for b may be caused by the observation and analysis techniques but also by the different wave conditions studied by the authors. For instance, *Duncan* [1981] observed steady breakers generated by an hydrofoil while *Banner and Peirson* [2007] surveyed transient breakers within wave groups. It also stresses a need for a better knowledge of the breaking dissipation process itself.

5.2. The Bore Model

[18] The bore model was initially used for predicting the energy dissipation in shallow water breaking waves. The momentum equation integrated over a control volume embracing the undisturbed, hydrostatic, upstream and downstream velocities which are uniform over the vertical (U_1 and U_2, respectively), combined with the mass conservation $Q = U_1h_1 = U_2h_2$, yields the energy dissipated per unit bore width [*Lamb*, 1932]

$$\epsilon_{bore} = \frac{1}{4}\rho_w g \frac{(h_2 - h_1)^3}{h_1 h_2} Q, \quad (15)$$

where h_1 and h_2 denote the upstream and downstream water depth, respectively. The extension of this approach to real breaking waves requires some assumptions [*LeMéhauté*, 1962; *Divoky et al.*, 1970; *Battjes and Janssen*, 1978; *Thornton and Guza*, 1983]. Starting with shallow water breakers, the difference $h_2 - h_1$ can easily be identified with the height H of the breaking wave [e.g., *Battjes and Janssen*, 1978]

$$H = h_2 - h_1. \quad (16)$$

The volume discharge per unit width Q for a wave propagating at the speed C is most easily approximated as $Q = Ch$ [*Hwang and Divoky*, 1970]. The dissipation rate per unit crest length for shallow water breakers is then given by [e.g., *Stoker*, 1957; *Battjes and Janssen*, 1978; *Thornton and Guza*, 1983]

$$\epsilon_{TG} = \frac{1}{4}\rho_w g \frac{(BH)^3}{h} C, \tag{17}$$

where the product $h_1 h_2$ has been approximated by the mean water depth h, and B is a breaker coefficient of order $O(1)$ [*Battjes and Janssen*, 1978; *Thornton and Guza*, 1983].

[19] In deep water the orbital velocities and the horizontal pressure gradient are no longer vertically homogeneous, and the dissipation rate is thus different from equation (17). Investigating wave breaking due to current gradients, *Chawla and Kirby* [2002] proposed to extend the bore model to deep water by assuming that the length scale h can be replaced by $\tanh(kh)/k$, with a limit $\lambda/2\pi$ in deep water (with λ the wavelength), and h in shallow water. This gives a dissipation rate per unit crest length

$$\epsilon_{CK} = \frac{1}{4}\rho_w g (BH)^3 \sqrt{\frac{gk}{\tanh(kh)}}. \tag{18}$$

Yet, this length scale h comes from the shallow water mass conservation and momentum equations which, as mentioned above, do not apply in deep water. In particular the energy fluxes are quadratic or cubic functions of the velocity profile and thus we may expect a stronger dependency on kh than $\tanh(kh)/k$ which corresponds to the vertical integration of a linear function of the velocity profile of linear waves. In fact, the expression by *Chawla and Kirby* [2002] systematically overestimates dissipation in deep water. We thus make a heuristic correction, replacing B by $B_{dw}/\tanh(kh)^p$, and we adjusted $p = 1.5$. This modification makes breaking relatively more severe in shallow water compared to deep water and the new breaking severity parameter $B_{dw}/\tanh(kh)^p$ may exceed unity as waves approaches very shallow water. Note that no upper bound is given in the literature, B being generally taken as a tunable constant of order 1 [*Battjes and Janssen*, 1978] and a function of the proportion of the foam region on the face of the breaker [*Thornton and Guza*, 1983].

[20] Our adjustment is rather arbitrary, and B, possibly depends on other parameters, as for instance, the beach slope. Although we do not have any detailed justification for the deep water transition of ϵ, the general decrease of ϵ appears indispensable when using our empirical breaking probabilities.

[21] We shall now attempt to estimate B_{dw}. In deep water, ϵ_{CK} tends to

$$\epsilon_{CK,dw} = \frac{1}{4}\rho_w B_{dw}^3 (kH)^3 \frac{C^5}{g}. \tag{19}$$

It is thus possible to compare it to ϵ_{Du}, given by equation (14)

$$\frac{\epsilon_{Du}}{\epsilon_{CK,dw}} = \frac{4b}{B_{dw}^3 (kH)^3}. \tag{20}$$

Duncan [1981] reported kH values around 0.67 for the deep water spilling breakers he recorded, thus, from $B_{dw} = (4b)^{1/3}/kH$ and from the different estimations of b found in the literature, we can estimate the order of magnitude of B_{dw}. As b was estimated between 8×10^{-5} and 0.045 this implies B_{dw} in the range 0.10–0.84. In the present study, the calibration yielded $B_{dw} = 0.185$.

6. Parameterizations of the Other Physical Processes

[22] The rest of the parameterizations is based on *Ardhuin et al.* [2010]. In that work, the air-sea interaction term contains a wind input adapted from the term initially proposed by *Janssen et al.* [1994] and adjusted by *Bidlot et al.* [2005, 2007], together with a negative part associated to a nonlinear swell dissipation [*Ardhuin et al.*, 2009, 2010]. In the present work, most of the model verifications are performed using the Discrete Interaction Approximation [*Hasselmann et al.*, 1985] for the nonlinear wave-wave interactions, except the tests of section 7.2, done with the exact interactions [*Webb*, 1978; *Tracy and Resio*, 1982] using the Webb-Resio-Tracy (WRT) algorithm for the exact nonlinear interactions, as implemented by *van Vledder* [2006].

[23] *Ardhuin et al.* [2010] found that the self-breaking source term S_{bk} is nonzero only when the nondimensional spectrum exceeds a threshold, consistent with observations [*Banner et al.*, 2000]. In the following, we shall replace that self-breaking term with the new parameterization presented above. Finally, the short-wave attenuation induced by large breakers sweeping the sea surface is given by *Ardhuin et al.* [2010].

7. Verification

7.1. Preliminary Calibrations

[24] The new source term has been implemented in the numerical wave model WAVEWATCH III [*Tolman*, 2002, 2008]. As explained in section 6, the new parameterization, called TEST500, is identical to TEST441b detailed by *Ardhuin et al.* [2010] except for the wave self-breaking dissipation S_{bk} that we have just described. For the sake of comparisons, we also use the parameterization by *Bidlot et al.* [2005, hereinafter BAJ]. Before running the model over complicated configurations, a preliminary calibration was done on a simple reference case. The model was run over a deep water, flat Earth uniform ocean, with a wind speed $U_{10} = 10$ m s^{-1} blowing over an infinite fetch and using 30 frequencies and 36 directions. The discrete interaction approximation [*Hasselmann et al.*, 1985], henceforth DIA, was used to represent the nonlinear interactions between the spectral components. Here we have used the fully developped sea state conditions, as parameterized by *Pierson and Moskowitz* [1964] and slightly revised by *Alves et al.* [2003] to calibrate $B_{dw} = 0.185$.

[25] In TEST441, the wave breaking dissipation is a function of the saturation spectrum and is thus local in frequency, which explains the sharp shape of the ocean source S_{oc} at the energy spectrum peak, where the saturation is maximum. This feature is found in both developing and fully developed seas (Figures 2 and 3). This shape is at odds with

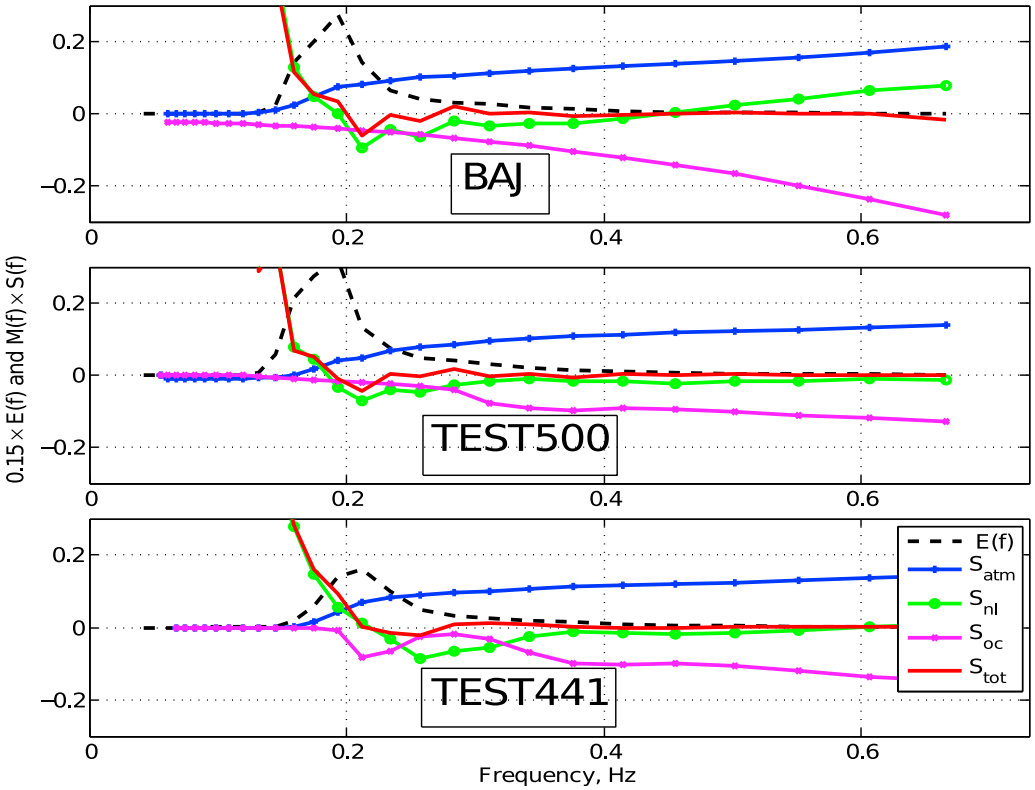

Figure 2. Spectrum and related source terms for an academic case, over a uniform ocean with a uniform 10 m s^{-1} wind starting from rest after 8 h of integration ($U_{10}/C_p \simeq 1$). The source terms are multiplied by the normalization function $M(f) = \rho_w C/(\rho_a E(f)\sigma U_{10})$, otherwise the spectrum level is not readable.

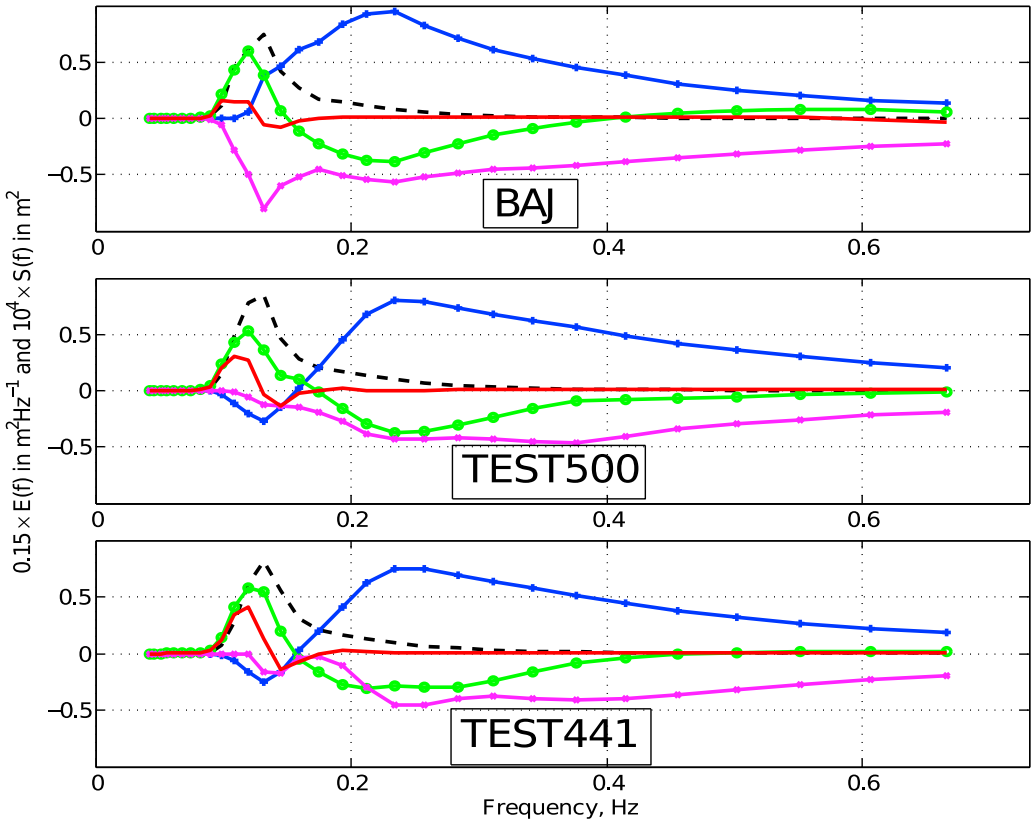

Figure 3. Same as Figure 2 but after 48 h of integration and without source term normalization.

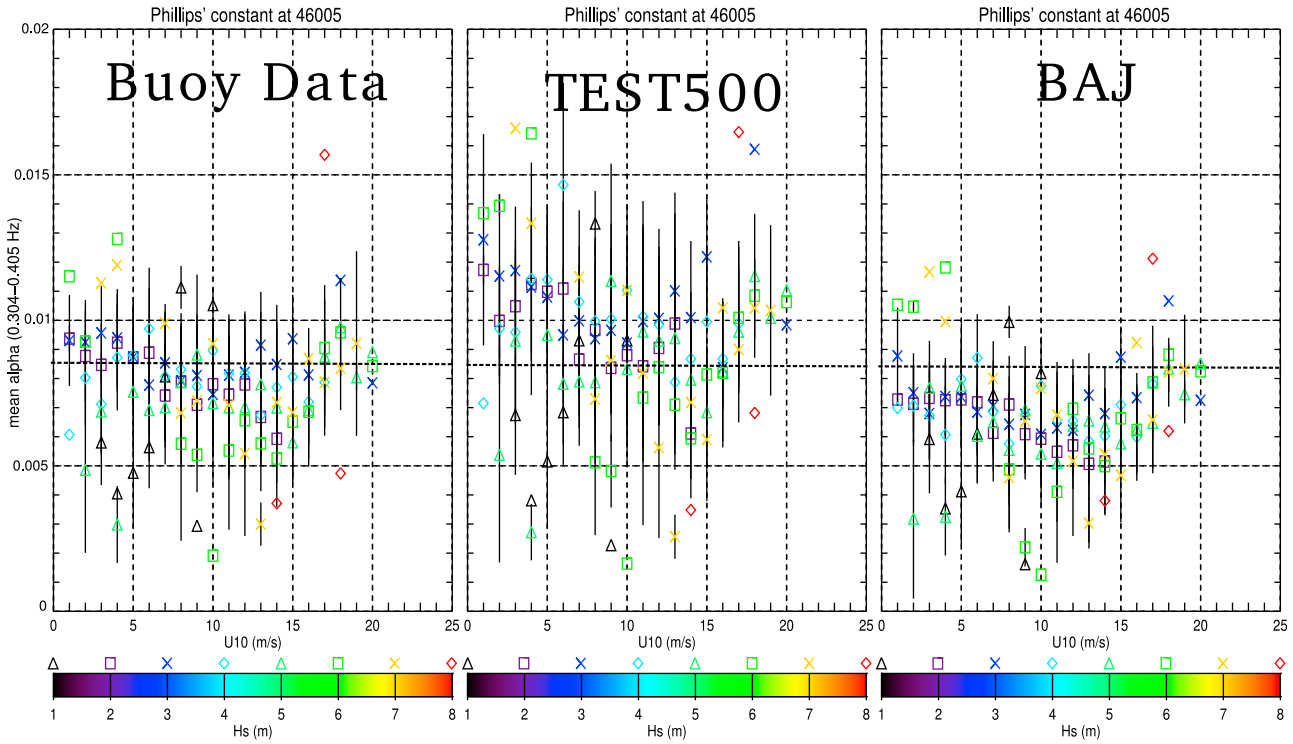

Figure 4. Nondimensional energy level at high frequency as a function of the 10 m high wind speed U_{10} and of the significant wave height H_s observed at National Data Buoy Center buoy 46005 for frequencies between 0.3 and 0.4 Hz during year 2007. (left) The observations and the results from (middle) TEST500 and (right) BAJ are shown. The Phillips constant (α = 7.4 10^{-3}) is shown by the horizontal black dashed line.

the nonlocal spectral nature of the breaking process. Indeed, the breaking dissipation occurs mostly within a finite duration τ, of the order of a wave period [*Rapp and Melville*, 1990], thus, the spectral components that contribute to a breaking wave cannot be distinguished within $\delta F \simeq 1/\tau$, as already noted by *Hasselmann* [1974]. Accordingly, in TEST500, the wave breaking dissipation is obtained from the spectrum filtered by our window $W_i(f)$.

[26] Figure 2 reveals that the dissipation (shown by S_{oc}) at high frequency is higher when using BAJ than TEST441 and TEST500. A major difference between BAJ, TEST441 and TEST500 resides in the spectral tail frequency dependence. In BAJ, as will be discussed in section 7.2, the spectrum is constrained to evolve like f^{-5} at high frequencies. In contrast, in TEST441 and TEST500 the spectral tail evolves freely. The behavior of the different parameterizations in the equilibrium range is illustrated by the spectral saturation in the tail region

$$\alpha = g^{-2}(2\pi)^4 f^5 E(f). \tag{21}$$

Figure 4 reveals that TEST500 tends to overestimate α and conversely, α is underestimated by BAJ. Due to uncertainties in buoy measurements above f = 0.4 Hz, we only consider frequencies below that value. The observations also suggest that the tail level decreases with wave age, consistently with the JONSWAP experiment observations. Finally, *Babanin and Soloviev* [1998] reported that α is constant in the earliest stage of wave development, a feature well captured by TEST500 (Figure 4).

7.2. Verification With an Exact Nonlinear Interactions Source Term

[27] The use of the DIA, is a common shortcoming of all the operational wave forecasting models [*van Vledder et al.*, 2000]. Although much less time-consuming, this approach is in general less accurate [e.g., *Banner and Young*, 1994; *Benoit*, 2005] than the exact methods [*Webb*, 1978; *Tracy and Resio*, 1982]. It is thus paramount for the future to investigate the behavior of TEST500 when run with the exact nonlinear interactions [*Webb*, 1978; *Tracy and Resio*, 1982] source term. Here we used the Webb-Tracy-Resio algorithm for the exact nonlinear interactions, hereinafter XNL, as coded by *van Vledder* [2006]. To maintain a reasonable energy level in the spectral tail, we apply a diagnostic tail (as done by BAJ), proportional to f^{-5} is imposed at a cutoff frequency f_c

$$f_c = r_{FM} f_m, \tag{22}$$

with $f_m = 1/T_{m0,1}$. Here, we take r_{FM} = 4.5 (r_{FM} = 2.5 is used in BAJ). This constraint allows an acceptable fit to frequency spectrum shape observations as shown in Figure 5. Figure 5 shows, for the mean direction, that results with the XNL source term are in slightly better agreement with observations, this is probably due to its greater ability to

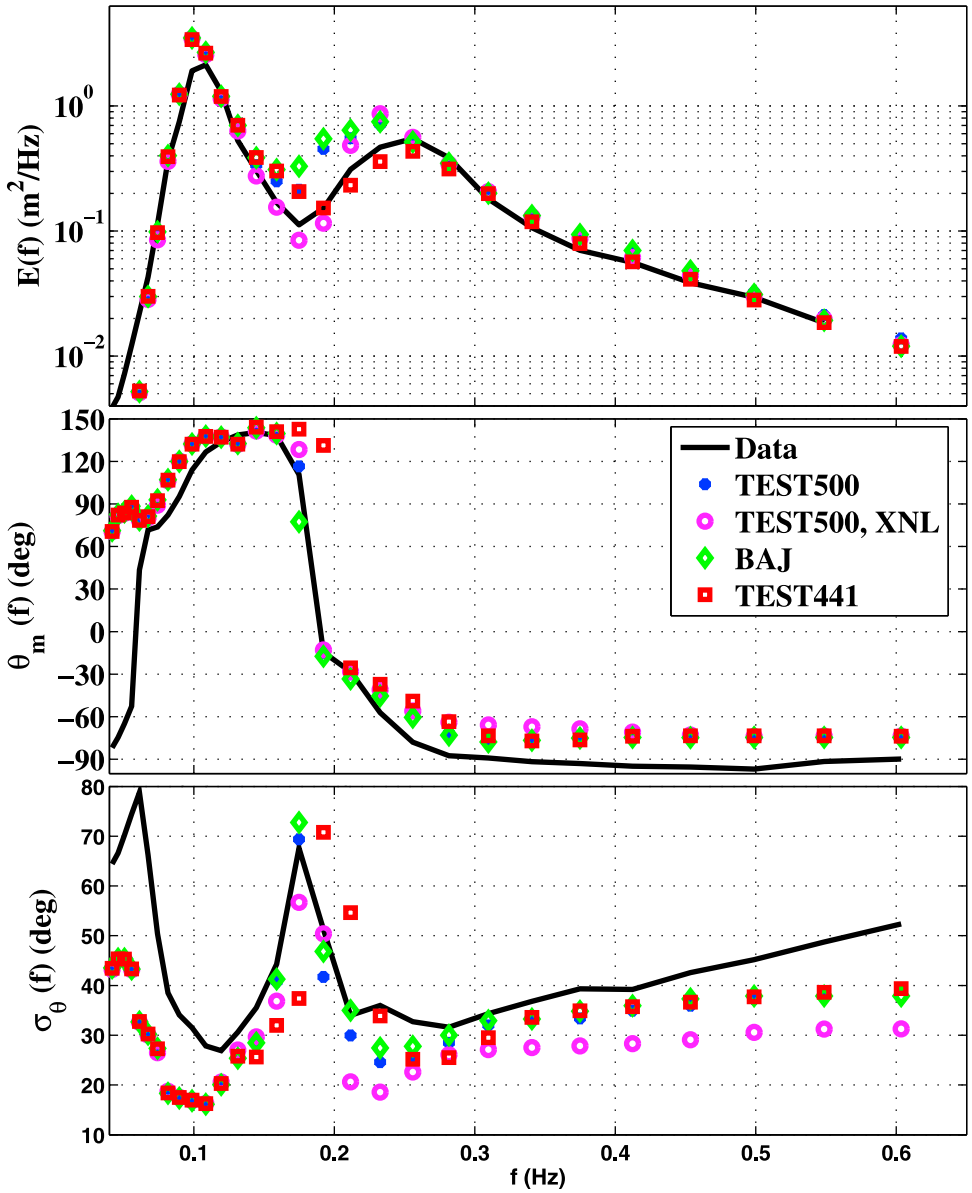

Figure 5. (top) Wave spectra, (middle) mean direction, and (bottom) directional spread on 3 November 1999 at buoy X3 (fetch 39 km, wind speed U_{10} = 9.4 m s^{-1}), averaged over the time window 1200–1700 LT, from observations (Shoaling Waves Experiment (SHOWEX)) and models runs with different model parameterizations. For further information on the SHOWEX experiment, see *Ardhuin et al.* [2003] (see Figure 2 for wave buoys location).

represent the "steering effect" caused by wave-wave interactions [*Bottema and van Vledder*, 2009; *Gagnaire-Renou*, 2010]. Note also that the shift between modeled and measured mean wave direction $\theta_m(f)$ (Figure 5, middle) at frequencies above 0.2 Hz are due to a bias of about 20° in direction of the wind fields used as input of the model. Furthermore, at high frequencies, the modeled directional spreads are significantly narrower than observed, especially when using the XNL source term. DIA is known to artificially broaden the spectrum. As a consequence, the wind input and dissipation source terms have been adjusted to correct this shortcoming. In the following we shall use the DIA and abandon the f^{-5} constraint.

7.3. Deep Water Verification

7.3.1. Comparison With Altimeter Data

[28] The significant wave heights produced by the different parameterizations over the global ocean will be here compared to observations collected by altimeters (Envisat, Geosat Follow-On (GFO), Jason) during the entire year 2007. The well-calibrated altimeter-derived H_s measurements [*Queffeulou and Fillon*, 2008] allow a comprehensive verification of the model efficiency in all sorts of wave conditions. The model was integrated over a uniform 0.5° resolution grid covering 80° South to 80° North. The very large number of along track-averaged altimeter observations (about 2 million) makes the results of this analysis very

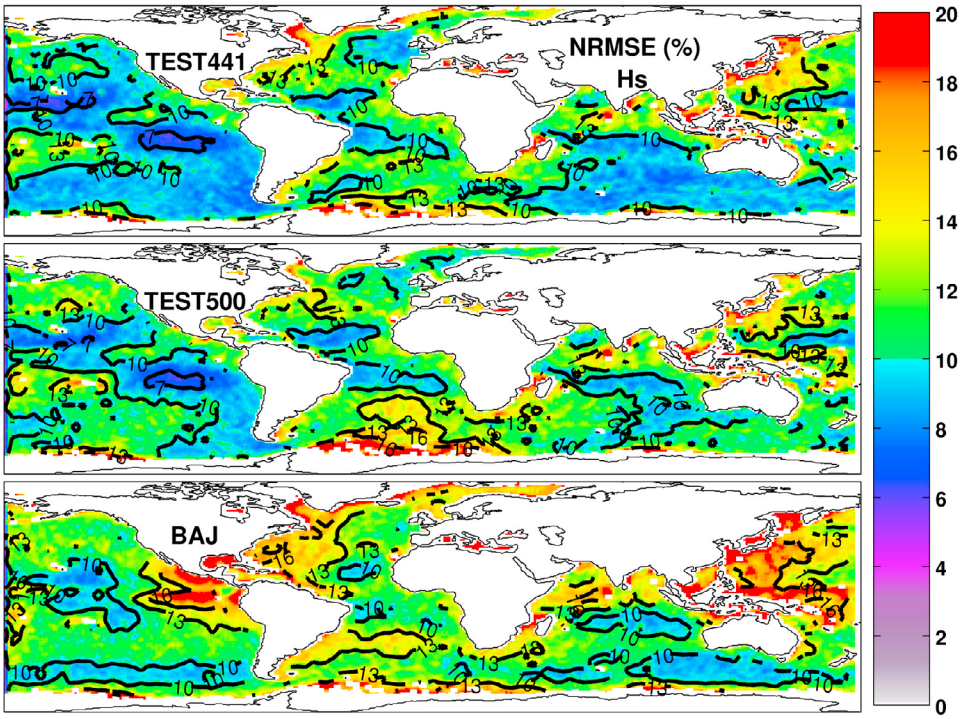

Figure 6. Comparison between significant wave height (H_s) fields produced by models and H_s derived from altimeter observations for the entire 2007 year. (top) NRMSE in percent for TEST441, (middle) NRMSE in percent for TEST500, and (bottom) NRMSE in percent for BAJ are shown.

robust. For the comparison of the models time series X_{mod} versus the observed time series X_{obs}, three statistics are used, the normalized root-mean-square error

$$\mathrm{NRMSE}(X) = \sqrt{\frac{\sum (X_{obs} - X_{mod})^2}{\sum X_{obs}^2}}, \tag{23}$$

the bias B

$$B(X) = \sqrt{\frac{\sum X_{obs} - X_{mod}}{N}}, \tag{24}$$

and the Scatter Index SI

$$\mathrm{SI}(X) = \frac{\sqrt{\frac{\sum (X_{obs} - X_{mod} - B(X))^2}{N}}}{\sum X_{obs}^2}, \tag{25}$$

where the overbar denotes the arithmetic average and N the number of observations.

[29] As shown by Figure 6, the normalized root-mean-square error (NRMSE) averaged over the globe equals 11.5% for TEST500, 11.9% TEST441 and 13.4% for BAJ. These first results are encouraging since the parameterizations TEST441 and BAJ generally provide the two most accurate results in global scale operational wave forecasting [e.g., *Bidlot*, 2008]. It is remarkable that compared to TEST441, TEST500 errors are stronger in the middle of the oceans. This higher error appears to be, in part, attributed to a too weak swell dissipation which has not been readjusted to the stronger swell sources in storms for TEST500. This is confirmed by the bias map (Figure 7) and by the Scatter Index (SI), which corresponds to the NRMSE corrected from the bias (Figure 8), and shows less differences between TEST441 and TEST500 in the middle of the oceans, particularly in the Pacific, compared to Figure 6. On the other hand, lower errors for TEST500 are observed in regions where waves are generally younger such as off the North East coast of the United States or off the South American East coast, or in the Mediterranean and North Seas. In the most probable wave conditions, namely for H_s between 1.5 meters and 7 meters TEST441 is more accurate (NRMSE about 10% versus 11% for TEST500) but interestingly, TEST500 significantly reduces the errors for high-wave conditions (Figure 9), with typical errors around 8–9% versus 11 to 13% for TEST441 (and BAJ). The Scatter Index (Figure 9) shows that most of the TEST441 and BAJ errors, for the high-waves conditions, are related to strong systematic negative biases. We note that for H_s larger than about 12 meters the altimeter measurements are not expected to be reliable due to the low backscatter and short waveform, and that ECMWF winds typically give weaker extreme winds than the NCEP analyses or reanalysis by *Saha et al.* [2010]. The behavior of ours and other model parameterizations at high winds will thus require further attention. Several case studies performed of storms generating significant wave heights larger than 14 m suggest that most of the low bias of the TEST441 parameterization forced by ECMWF winds is actually due to a bias in the forcing wind fields [*Ardhuin et al.*, 2011b]. Also we note that the large positive bias in the South Atlantic is well explained by the absence of iceberg parameterization in the model used here [*Ardhuin et al.*, 2011a].

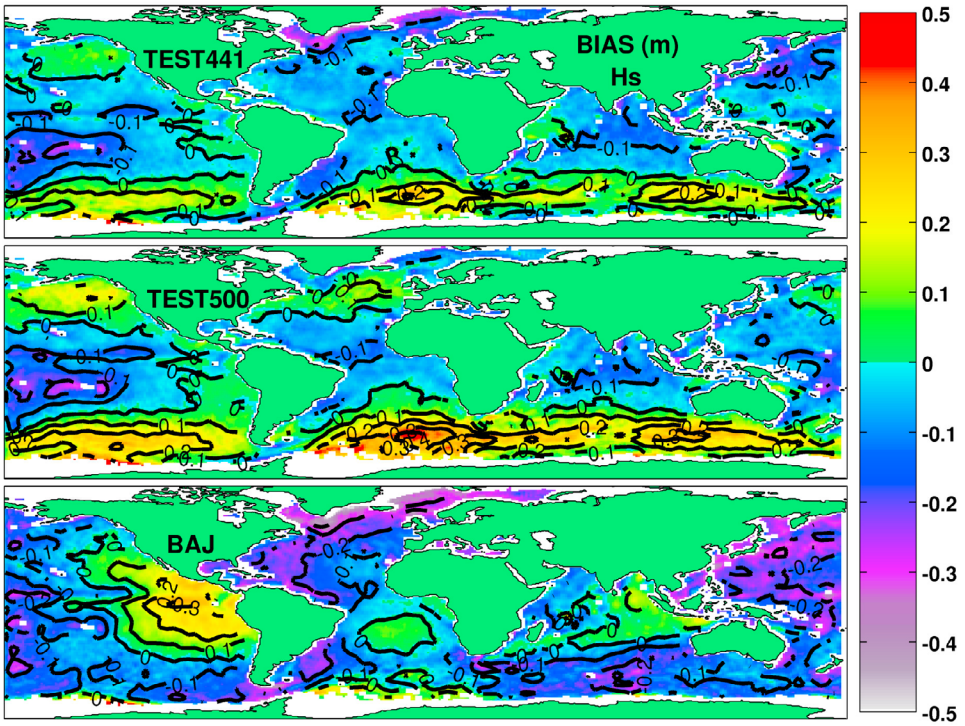

Figure 7. Same as Figure 6 but for the bias in meters.

7.3.2. Comparison With Buoy Measurements

[30] The same global model is also validated with observations from buoys of the U.S. National Data Buoy Center, U.K. Met. Office and Meteo France. A sample of buoys representative of different wave climates (young/old seas, presence/absence of long-period swell) have been used here. In addition to the wave height validation, this data set provides a verification of peak (T_p) or mean ($T_{m0,2}$) wave periods prediction (see Figures 10 and 11), depending on the data available from the buoys. For the wave heights and wave period, the NRMSE averaged over the set of buoy data are (12.1%, 16.6%) for TEST441, (12.9%, 19.2%) for

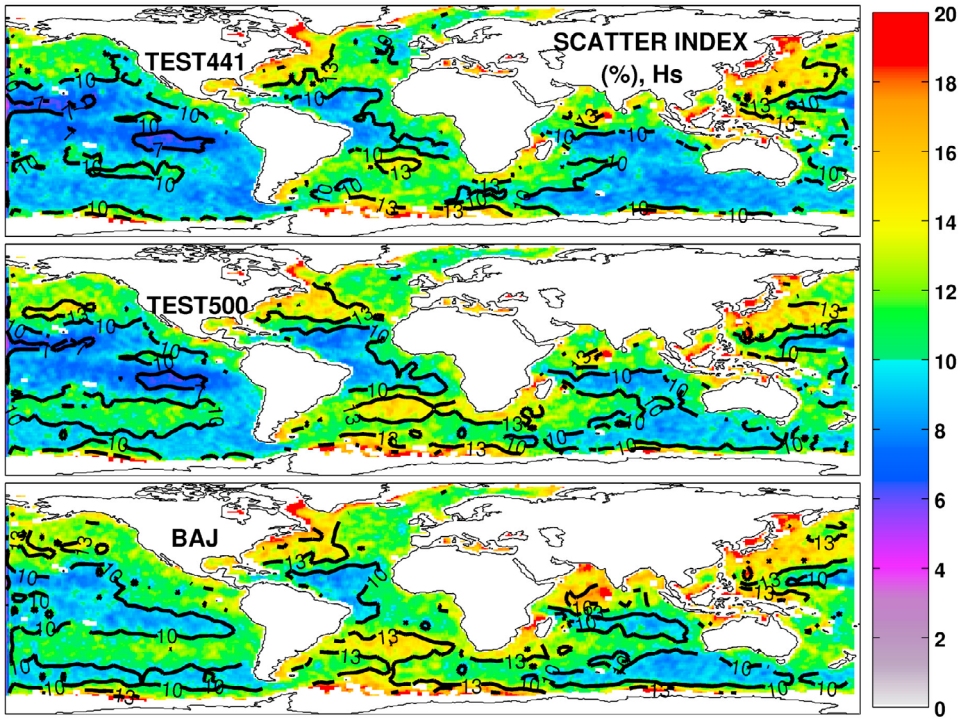

Figure 8. Same as Figure 6 but for the Scatter Index.

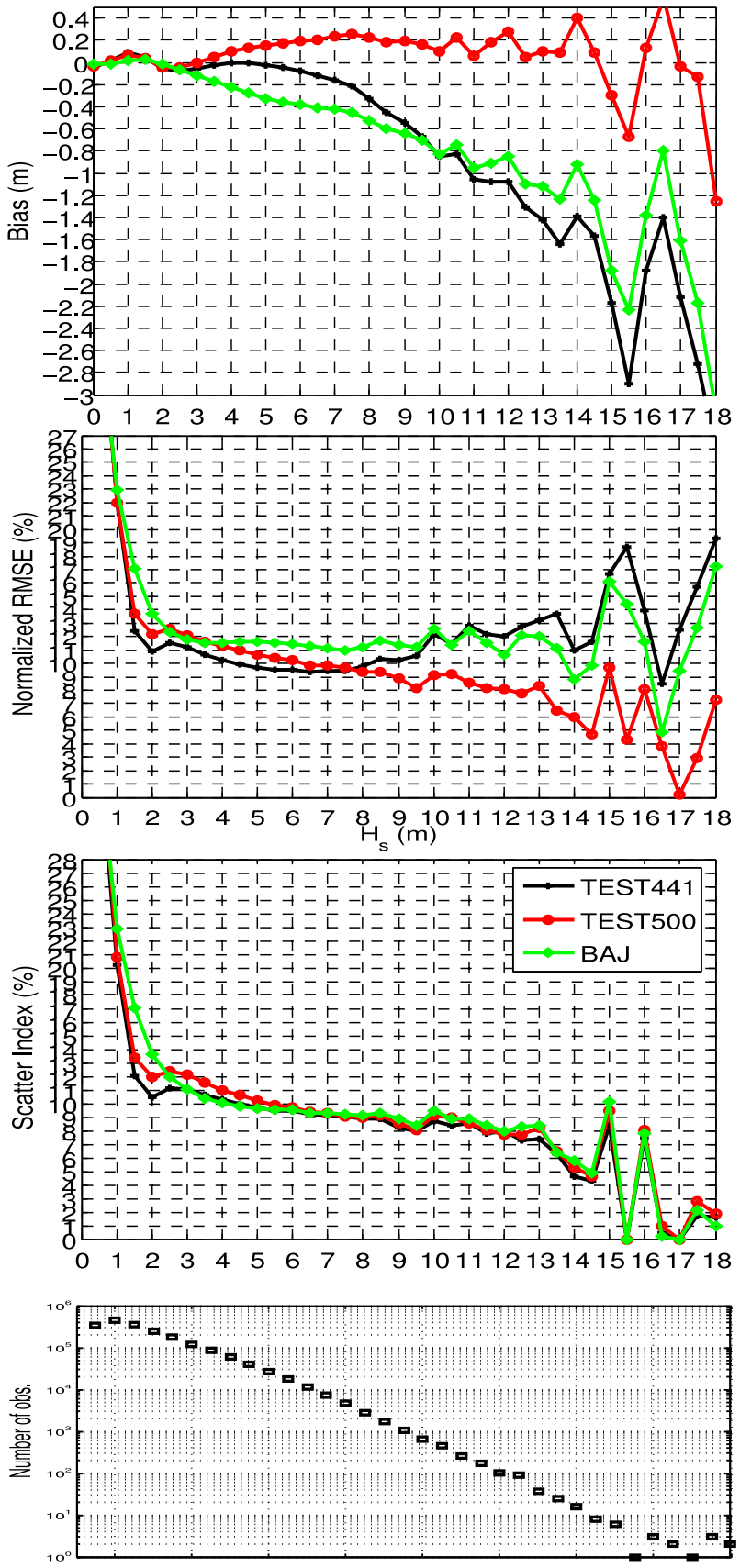

Figure 9. Wave model errors as a function of H_s. The model output at 3 h intervals is compared to Jason, Envisat, and GFO following the method of *Rascle et al.* [2008]. Namely the altimeter 1 Hz Ku band estimates of H_s are averaged over 1°.

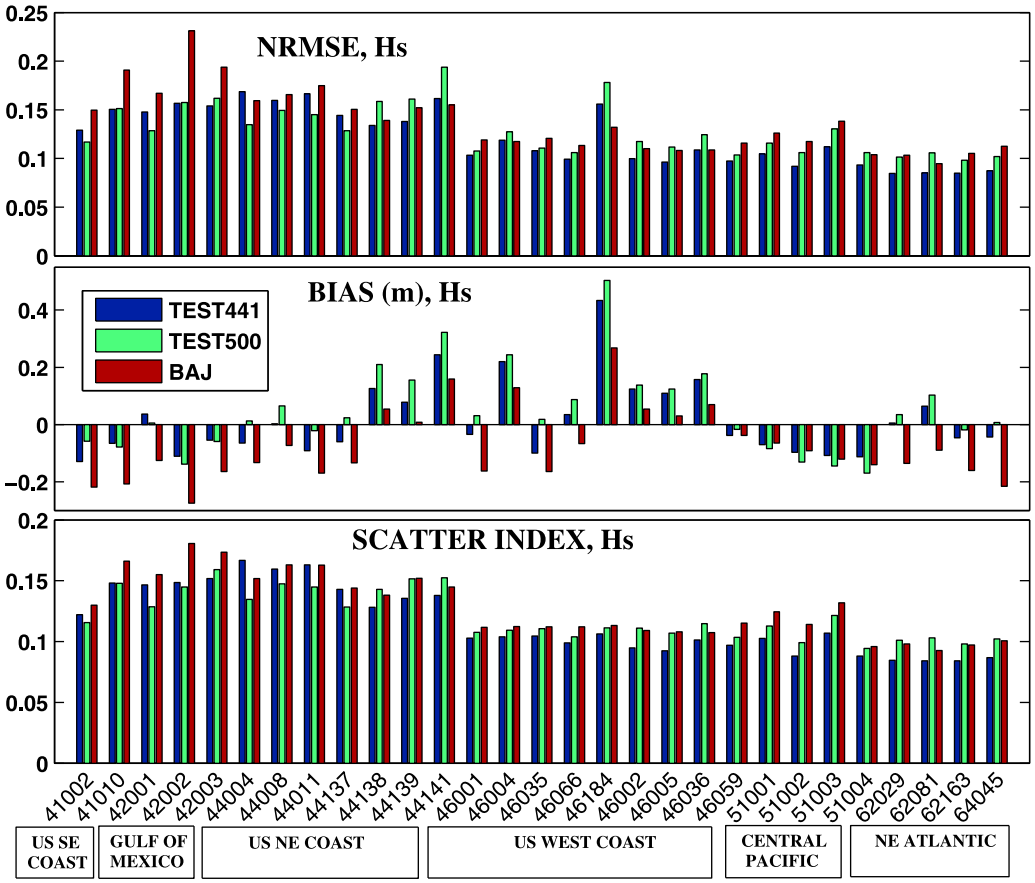

Figure 10. Comparison to buoys measurements for the significant wave height. The bottom x axis shows the different buoys used for this verification. Their regional positions are shown below for convenience. (top) The NRMSE for the three parameterizations, (middle) the bias in meters, and (bottom) the Scatter Index relative to the buoy observations are shown.

TEST500 and (13.7%, 21.9%) for BAJ, respectively. These results and those of the altimeter comparison are summed up in Table 2. TEST500 wave period predictions are less accurate (compare to TEST441) in the middle of the oceans (West Coast of the United States and Central Pacific), further recalibrations of the wind input, cumulative dissipation or swell attenuation terms might correct these errors.

7.4. Depth-Induced Breaking Conditions

[31] The most challenging objective of our work was to show that it is possible to represent the breaking-induced dissipation in all water depths with a single parameterization. The exact same settings as in the global model are used and tested with two shallow water data sets provided by Steve Elgar of Woods Hole Oceanographic Institution and Gerben Ruessink of Utrecht University. The first data were collected during the Duck94 experiment at the U.S. Army Corps of Engineers Field Research Facility (FRF). For details about the experiment one may read the presentations by *Elgar et al.* [1997], *Gallagher et al.* [1998], and *Feddersen et al.* [1998]. The root-mean-square wave height is defined by $H_{rms} = H_s/\sqrt{2}$ and was estimated from instruments installed from the shoreline as far as across the subtidal bar. Wave observations from a triple barred beach at Terschelling island, Netherlands [*Ruessink et al.*, 1998], were also employed. The depth profiles are displayed on Figure 12 and the offshore conditions are summarized in Table 3.

[32] In both cases, observed offshore boundary energy spectra were used to force the model in time. A 5 m resolution grid was used along with global, propagation and source terms time steps set to 0.2 seconds. The direction resolution was 15° and 32 frequency bins were used, ranging from 0.0373 Hz to 0.7875 Hz. Also, for both experiments, the bathymetry was measured repeatedly and this temporal evolution has been taken into account in our numerical simulations. As a reference was required to judge the efficiency of the new parameterization, we additionally ran the TEST441 model, using the *Battjes and Janssen* [1978] breaking induced source term (with $\gamma = 0.73$), widely used to represent the spectral depth-induced breaking dissipation. *Battjes and Janssen* [1978] estimated the breaking-induced energy dissipation δ from the turbulent bore model. The related spectral source term assumes an uniform distribution of δ over the energy spectrum. Figures 13 and 14 show the comparison of the models results in terms of wave height with observations collected at different points of the cross-shore profile. Both models achieve a good fit to observations. The performances of both source terms are comparable for the Terschelling case with a slight advantage to the parameterization of Battjes and Janssen (see Figure 15, NRMSE = 11% versus 12% for TEST500). For the Duck case, the

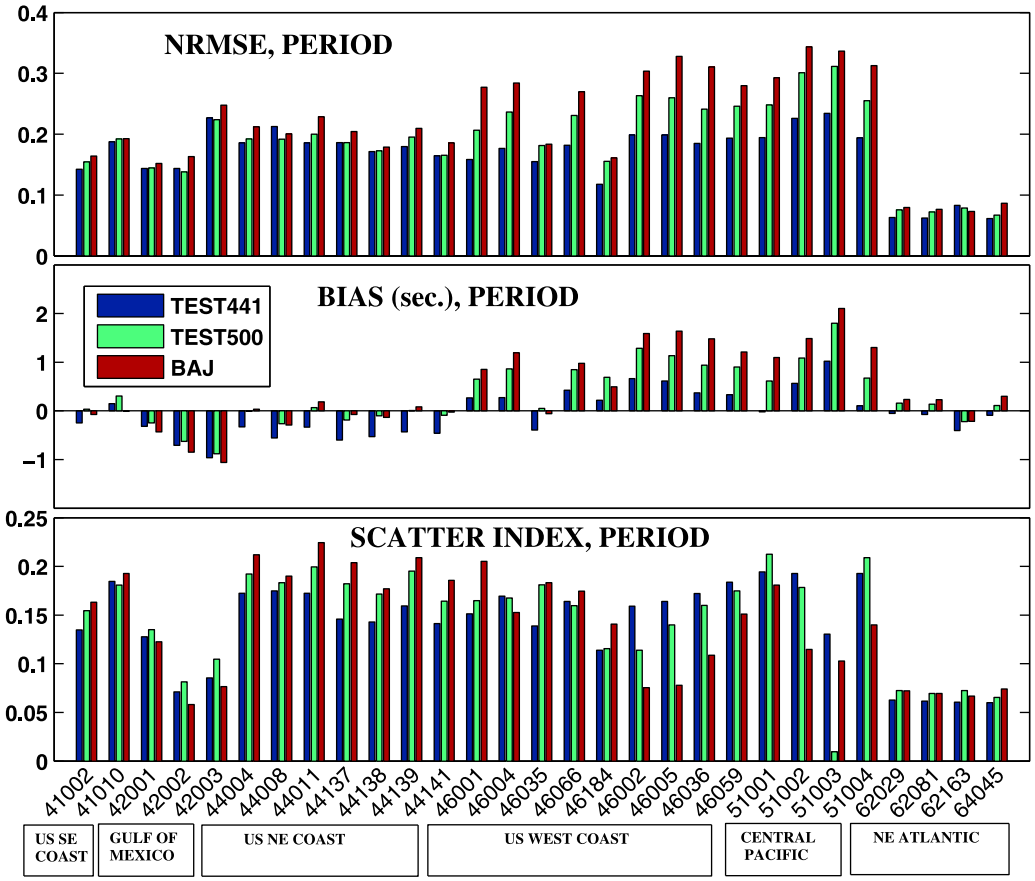

Figure 11. Same as Figure 10 but for the peak or mean period $T_{m0,2} = \left[\int_0^{2\pi}\int_0^{f_{max}} f^2 E(f,\theta) df\, d\theta\right]^{1/2}$, f_{max} is set to 0.5 Hz for the model results and is expected to be about 0.4–0.5 Hz for the buoy data. For the last four buoys the mean period is used for the comparison, whereas for all others buoys the peak period is used.

scatterplot in Figure 16 suggests however that TEST500 better agrees with the observations, with an NRMSE and a bias of about 12% and 0.04m versus 20% and 0.1m, respectively, for Battjes and Janssen's source term.

[33] It has been stressed by several authors [e.g., *Miche*, 1944; *Stive*, 1984; *Svendsen*, 1984] that the shallow water breaking limit γ is a function of the beach slope [e.g., *van der Westhuysen*, 2010] and of *kh*. *Ruessink et al.* [2003] performed a careful analysis of depth-induced breaking data and proposed the following parameterization for γ:

$$\gamma = 0.76kh + 0.29 \tag{26}$$

that allows significant improvements in the model results. This parameterization was not considered here. It is nonetheless worth noting that for $kh < 0.3$, The approach of FAB is consistent with the findings of *Ruessink et al.* [2003] since, in shallow water, $\beta_{t,\,\mathrm{lin}}$ corresponds to a γ varying with water depth [*Filipot et al.*, 2010].

[34] The ability of the parameterizations to reproduce spectral shapes was investigated over approximately a tidal cycle at point T3, for the Terschelling data set. The observed spectra were deduced from pressure measurements and this study suggests that both models tend to overestimate the energy at the spectral peak. This discrepancy is less marked for TEST500 especially under strong breaking conditions (occurring at low tides, see Figure 17). We additionally verified that the frequency dependence of the normalized breaking dissipation ($S_{bk}(f)/E(f)$) produced by our model agrees with the f^2 dependence observed by *Elgar et al.* [1997] over depth-induced breaking conditions (not shown here). A comparison of the modeled and observed peak period was also performed (not presented in this paper) and shows similar results between TEST500 and Battjes and Janssen term. Both models tend nonetheless to give periods that are slightly too large. This is a well know defect of models that only consider linear wave dispersion and can be corrected by parameterizing the growth of harmonics in shallow water [e.g., *Eldeberky and Battjes*, 1996; *Janssen*, 2009].

Table 2. Normalized Root-Mean-Square Error for H_s and T_p for the Altimeter (Global) and Buoy Comparisons[a]

	NRMSE (%)		
	H_s, Global	H_s, Buoys	T_p, Buoys
BAJ	13.4	13.7	21.9
TEST441	11.2	12.1	16.6
TEST500	11.9	12.9	19.2

[a]Each line corresponds to a model.

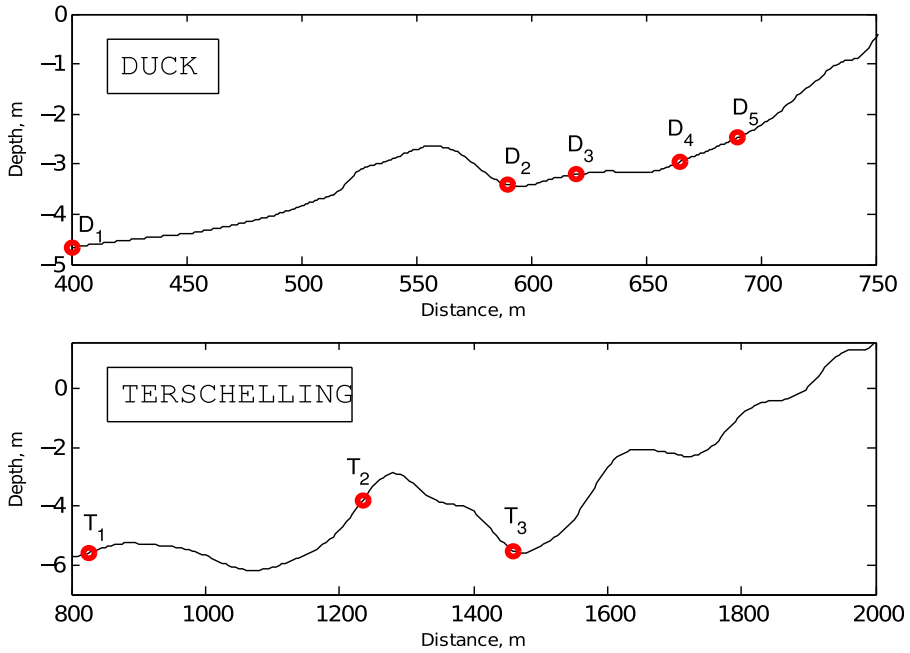

Figure 12. Bathymetry profiles (black line) and measurement points (red circles) for the (top) Duck case and the (bottom) Terschelling case.

[35] Also, the present parameterization for the breaking probability Q_B yields values greater than unity during high-wave events. In shallow water, apart from the spectral dependence, our breaking probability tends to the parameterization of [*Thornton and Guza*, 1983] that may locally exceed unity, as shown by *Janssen and Battjes* [2007] for wave breaking over steep beaches. Such fundamental issues will certainly be the topic of further investigations.

8. Conclusions

[36] This work has shown that it is possible to represent the breaking dissipation from the deep ocean to the surf zone by a single term based on a carefully calibrated parameterization for the probability density of breaking waves [*Filipot et al.*, 2010]. The key ingredient in this was a depth-dependent dissipation rate per unit length of breaking front. This dissipation rate is of the order of reported observations, however the large scatter in these observations does not guarantee the accuracy of our parameterization. Although most of the tests were performed with the DIA parameterization of the nonlinear interactions, it is worth noting that our new parameterization also gives reasonable results when used with the exact formulation, provided a high-frequency tail is prescribed. In deep water, the new source term produces results comparable to those of the best operational wave forecasting models while in shallow water it performs better than the classical parameterization by *Battjes and Janssen* [1978]. For high-wave conditions, which are of particular interest for numerous applications, this parameterization was even shown to significantly improve the predictions.

[37] Further calibrations should allow appreciable improvements in the predictions, in particular in intermediate water where we expect that the usual combination of deep and shallow water breaking formulations produces insufficient dissipation because the depth-induced steepening is not fully included in the deep water term and the water is too deep for the "depth-limited" breaking to be active. Also, the importance of the directionality has, so far, not been taken into account by lack of knowledge, however, progress in wave measurement techniques [e.g., *Benetazzo*, 2006] should provide more information in the near future.

Appendix A: Practical Implementation of the Model

A1. Model Summary

[38] Additional technical details and a summary of the model are provided here. First we recall that a wave scale centered on f_i covers the frequency bandwidth $f_{i,-} = 0.7f_i$ to $f_{i,+} = 1.3f_i$. Sliding a rectangular window $W_i(f)$ along the frequency axis gives a range of N scales, where N is slightly less than M, the amount of frequencies in the model, since we take $f_{N,+} = f_M$. For each wave scale, a representative wave height H_r and wave number $\bar{k}_r$ are estimated

$$H_r(f_i) = \frac{4}{\sqrt{2}}\sqrt{\int_0^\infty W_i(f)E(f)df}, \tag{A1}$$

$$\bar{k}_r(f_i) = \frac{\int_0^\infty W_i(f)k(f)E(f)df}{\int_0^\infty W_i(f)E(f)df}. \tag{A2}$$

Table 3. Offshore Conditions Observed During the Experiments[a]

Site	H_{rms} (m)	T_p (s)	$\bar{\theta}$ (deg)	N
Duck	0.29–2.19	4.5–7.0	−30 to 50	270
Terschelling	0.12–1.83	3.0–12.8	−30 to 30	816

[a]N is the number of observations.

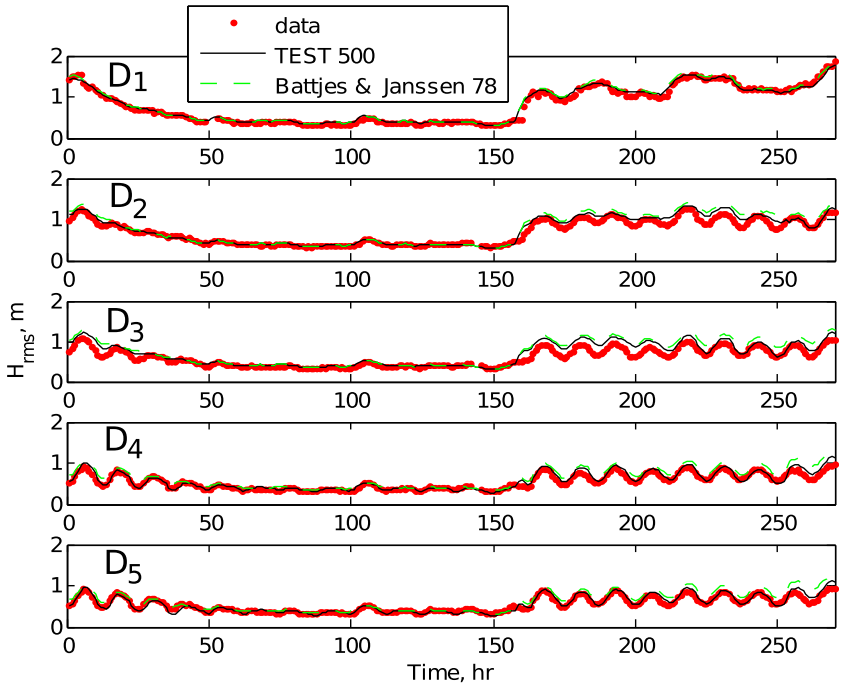

Figure 13. Comparison of observed spectrally derived root-mean-square wave height (H_{rms}) to modeled H_{rms} for the Duck94 case. Each figure presents a comparison of observed and modeled H_{rms} at one of the station (D1, D2, D3, D4, D5) indicated on Figure 12 (top).

A dissipation rate per unit area for any wave scale can further be obtained as

$$D(f_i) = Q(f_i) \times \epsilon(f_i) \times \Pi(f_i), \tag{A3}$$

with the dissipation rate per unit crest length $\epsilon(f_i)$, the crest length density per unit area $\Pi(f_i)$ and the breaking probability $Q(f_i)$, given as follows:

$$\epsilon(f_i) = \frac{1}{4}\rho_w g \left(\frac{B_{dw} H}{\tanh(k(f_i)h)^p}\right)^3 \sqrt{\frac{gk(f_i)}{\tanh(k(f_i)h)}}, \tag{A4}$$

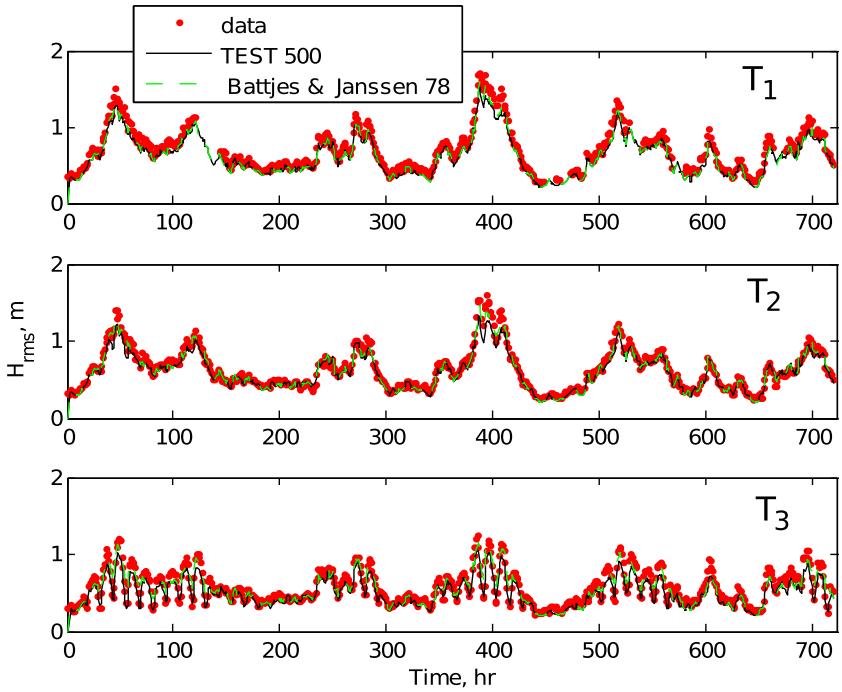

Figure 14. Same as Figure 13 but for the Terschelling data set. Each figure presents a comparisons of observed and modeled H_{rms} at one of the station (T1, T2, T3) indicated on Figure 12 (bottom).

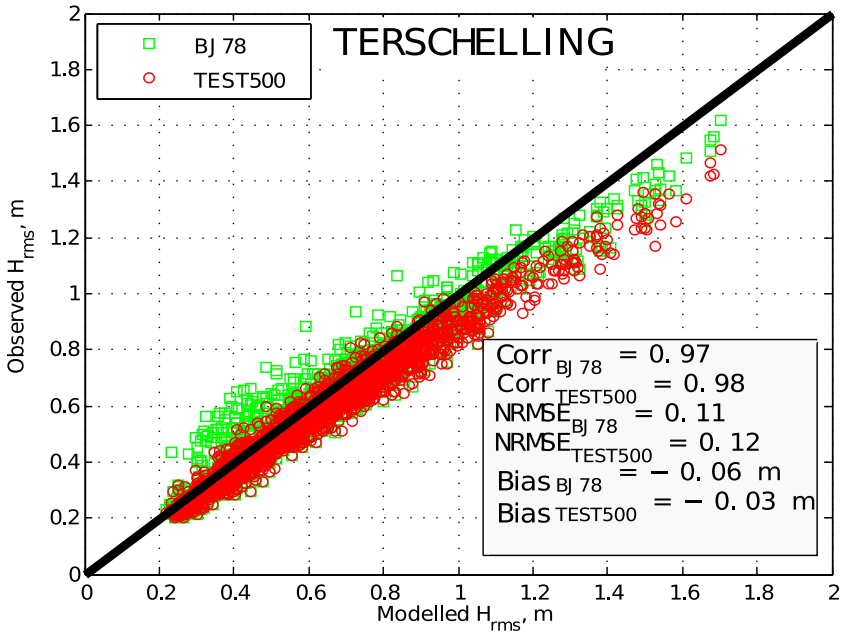

Figure 15. Scatterplot of the modeled H_{rms} (green squares are Battjes and Janssen term and red circles are TEST500) versus observed H_{rms} for the Terschelling case. This comparison involves the H_{rms} values of all stations (T1, T2, T3). The correlation, NRMSE, and bias are shown.

$$\Pi(f_i) = \frac{k(f_i)}{2\pi}, \tag{A5}$$

$$Q_B(f_i) = \int_0^{\infty} P_B(f_i, H) dH. \tag{A6}$$

The broken wave heights probability density is further defined as

$$P_B(f_i, H) = 1.5\left[\frac{\beta_r}{\beta_{t,\mathrm{lin}}}\right]^2 \left\{1 - \exp\left[-\left(\frac{\beta}{\beta_{t,\mathrm{lin}}}\right)^4\right]\right\} \cdot \frac{2H}{H_r^2(f_i)} \exp\left(-\left(\frac{H}{H_r(f_i)}\right)^2\right). \tag{A7}$$

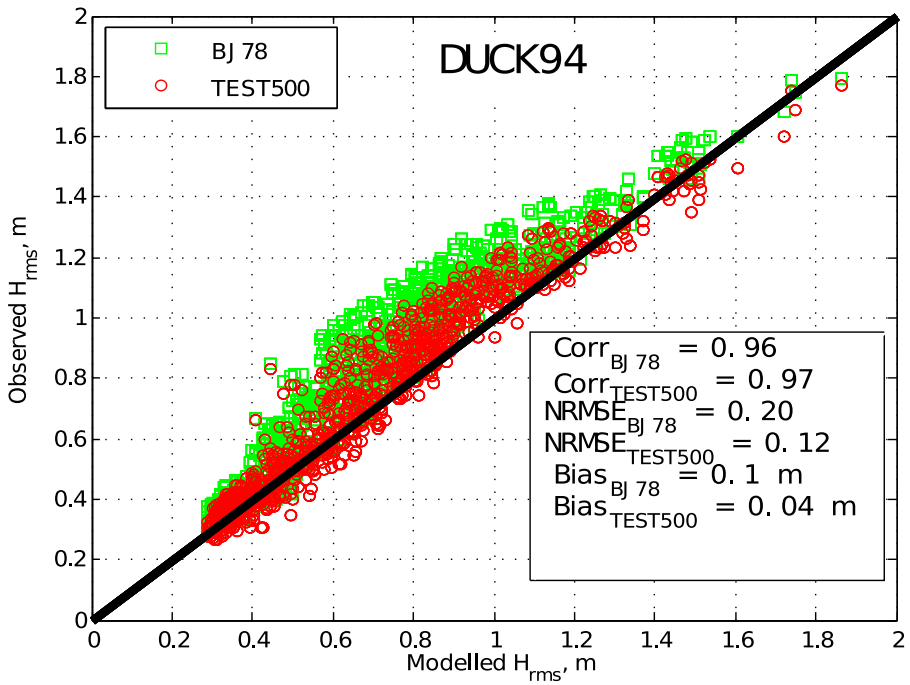

Figure 16. Same as Figure 15 but for the DUCK94 case. This comparison involves the H_{rms} values of all stations (D1, D2, D3, D4, D5).

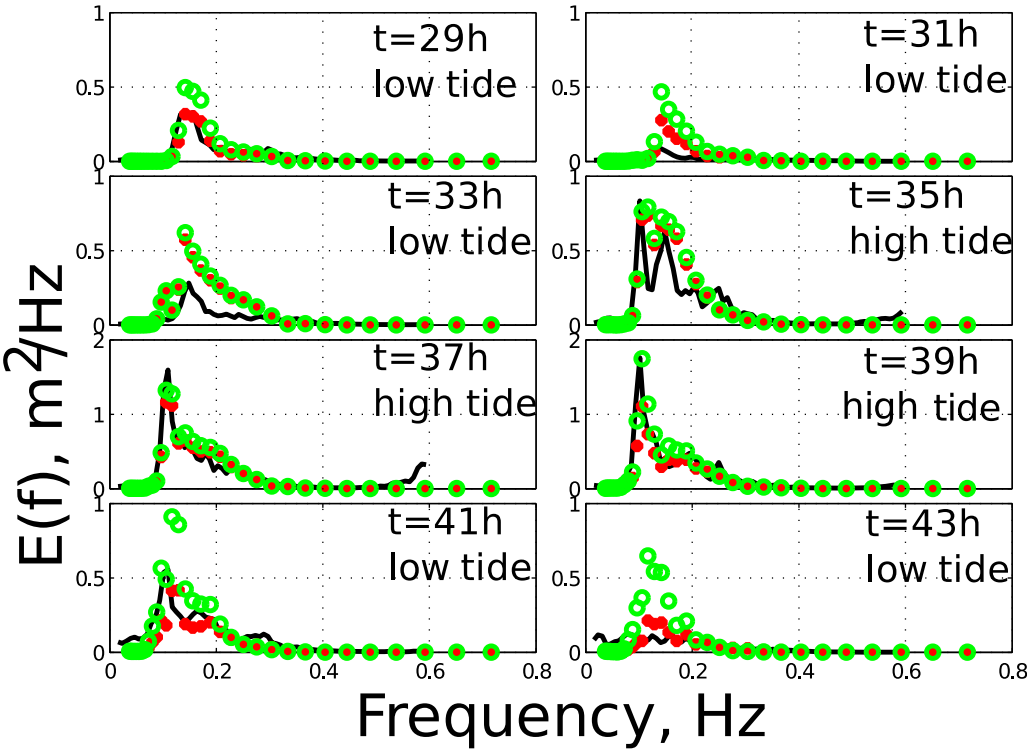

Figure 17. Frequency spectra at T3 for the period 29–43 h. The black lines show the pressure-derived spectra, the red points give the spectra produced by TEST500, and the green circles show the results when using the *Battjes and Janssen* [1978] term.

As the chosen dissipation rate per unit crest length ϵ is a function of the broken wave height, $D(f_i)$ now writes

$$D(f_i) = \Pi(f_i) \times \int_0^\infty P_B(f_i, H)\epsilon(f_i, H)dH. \quad \text{(A8)}$$

The distribution of $D(f_i)$ over the spectral components contributing to the scale f_i is simply achieved through weighting $D(f_i)$ by the spectral densities falling in the proper range (prescribed here by the rectangular window $W_i(f)$)

$$S_{bk,i}(f) = \frac{D(f_i) \times E(f)}{\int_0^\infty E(f)W_i(f)df}. \quad \text{(A9)}$$

Finally, because each spectral component f is associated with several wave scales, from f_j to f_k the final source term is expressed as

$$S_{bk}(f) = \frac{1}{k-j+1}\sum_{i=j}^{k} S_{bk,i}(f). \quad \text{(A10)}$$

A2. Precisions on the Numerical Implementation

[39] For practical reasons, in the implemented model, the scale f_i involves frequencies in the range $f_{i,-} = f_i$ to $f_{i,+} = (1.3/0.7)f_i$. Note that this arbitrary convention has no effect on the results. In addition, to shorten the computational time, D is tabulated at the first model time step as a function of kh and kH_r. Then, at each time step and grid point, and for each wave scale f_i, $k(f_i)h$ and $k(f_i)H_r(f_i)$ are estimated and the corresponding value of $D(f_i)$ is sought in the precalculated lookup table. Finally, equations (35) and (36) are solved to give the final spectral dissipation rate $S_{bk}(f)$.

[40] **Acknowledgments.** J.-F.F. acknowledges the support of a CNRS-DGA doctoral research grant; F.A. is supported by grants 240009 "IOWAGA" from the European Research Council and N00014-10-1-0383 from the U.S. Office of Naval Research, via the National Ocean Partnership Program. Fields observations provided by Steve Elgar were funded by the U.S. Office of Naval Research. The authors thank Gerben Ruessink for his assistance in using the Duck and Terschelling observations.

References

Agrawal, Y. C., E. A. Terray, M. A. Donelan, P. A. Hwang, A. J. Williams, W. Drennan, K. Kahma, and S. Kitaigorodskii (1992), Enhanced dissipation of kinetic energy beneath breaking waves, *Nature*, *359*, 219–220.

Alves, J. H. G. M., M. L. Banner, and I. R. Young (2003), Revisiting the Pierson-Moskowitz asymptotic limits for fully developed wind waves, *J. Phys. Oceanogr.*, *33*, 1301–1323.

Ardhuin, F., T. H. C. Herbers, P. F. Jessen, and W. C. O'Reilly (2003), Swell transformation across the continental shelf. Part II: Validation of a spectral energy balance equation, *J. Phys. Oceanogr.*, *33*, 1940–1953.

Ardhuin, F., B. Chapron, and F. Collard (2009), Observation of swell dissipation across oceans, *Geophys. Res. Lett.*, *36*, L06607, doi:10.1029/2008GL037030.

Ardhuin, F., et al. (2010), Semi-empirical dissipation source function for wind-wave models: Part 1. Definition, calibration and validation at global scales, *J. Phys. Oceanogr.*, *40*(9), 1917–1941.

Ardhuin, F., J. Tournadre, P. Queffelou, and F. Girard-Ardhuin (2011a), Observation and parameterization of small icebergs: Drifting breakwaters in the Southern Ocean, *Ocean Modell.*, *39*, 405–410.

Ardhuin, F., J. Hanafin, Y. Quilfen, B. Chapron, P. Queffeulou, M. Obrebski, J. Sienkiewicz, and D. Vandemark (2011b), Calibration of the iowaga global wave hindcast using ECMWF and CFSR winds, paper presented at 12th International Workshop of Wave Hindcasting and Forecasting, Environ. Can., Kohala Coast, Hawaii, 30 Oct. to 4 Nov.

Babanin, A. V. (2009), Breaking of ocean surface waves, *Acta Phys. Slovaca*, *59*, 305–535.

Babanin, A. V., and Y. P. Soloviev (1998), Field investigation of transformation of the wind wave frequency spectrum with fetch and the stage of development, *J. Phys. Oceanogr.*, *28*, 563–576.

Banner, M. L., and R. P. Morison (2010), Refined source terms in wind wave models with explicit wave breaking prediction. Part I: Model framework and validation against field data, *Ocean Modell.*, *33*, 177–189, doi:10.1016/j.ocemod.2010.01.002.

Banner, M. L., and W. L. Peirson (2007), Wave breaking onset and strength for two-dimensional deep-water wave groups, *J. Fluid Mech.*, *585*, 93–115.

Banner, M. L., and I. R. Young (1994), Modeling spectral dissipation in the evolution of wind waves. Part I: Assessment of existing model performance, *J. Phys. Oceanogr.*, *24*(7), 1550–1570.

Banner, M. L., I. S. F. Jones, and J. C. Trinder (1989), Wavenumber spectra of short gravity waves, *J. Fluid Mech.*, *198*, 321–344.

Banner, M. L., A. V. Babanin, and I. R. Young (2000), Breaking probability for dominant waves on the sea surface, *J. Phys. Oceanogr.*, *30*, 3145–3160.

Battjes, J. A., and J. P. F. M. Janssen (1978), Energy loss and set-up due to breaking of random waves, in *Proceedings of the 16th International Conference on Coastal Engineering*, edited by Coastal Engineering Research Council, pp. 569–587, Am. Soc. of Civ. Eng., New York.

Benetazzo, A. (2006), Measurements of short water waves using stereo matched images sequences, *Coastal Eng.*, *53*, 1013–1032.

Benoit, M. (2005), Evaluation of methods for the computation of nonlinear four-wave interactions in discrete spectral wave models, paper presented at 5th International Symposium Ocean Wave Measurement and Analysis, Am. Soc. of Civ. Eng., Madrid, 3–7 Jul.

Bidlot, J.-R. (2008), Intercomparison of operational wave forecasting systems against buoys: Data from ECMWF, Metoffice, FNMOC, NCEP, DWD, BoM, SHOM and JMA, September 2008 to November 2008, technical report, Joint Tech. Comm. for Oceanogr. and Mar. Meteorol., World Meteorol. Organ.-Int. Oceanogr. Comm., Geneva, Switzerland.

Bidlot, J., S. Abdalla, and P. Janssen (2005), A revised formulation for ocean wave dissipation in CY25R1, *Tech. Rep. Memo. R60.9/JB/0516*, Res. Dep., Eur. Cent. for Medium-Range Weather Forecasts, Reading, U. K.

Bidlot, J., P. Janssen, and S. Abdalla (2007), A revised formulation of ocean wave dissipation and its model impact, *Tech. Rep. Memo. 509*, ECMWF, Reading, U. K.

Bottema, M., and G. P. van Vledder (2009), A ten-year data set for fetch- and depth-limited wave growth, *Ocean Modell.*, *57*(7), 703–725.

Chawla, A., and J. T. Kirby (2002), Monochromatic and random wave breaking at blocking points, *J. Geophys. Res.*, *107*(C7), 3067, doi:10.1029/2001JC001042.

Cointe, R., and M. P. Tulin (1994), A theory of steady breakers, *J. Fluid Mech.*, *276*, 1–20.

Divoky, D., B. Le Mehaute, and A. Lin (1970), Breaking waves on gentle slopes, *J. Geophys. Res.*, *75*, 1681–1692.

Duncan, J. H. (1981), An experimental investigation of breaking waves produced by a towed hydrofoil, *Proc. R. Soc. London A*, *377*, 331–348.

Duncan, J. H. (1983), The breaking and non-breaking wave resistance of a two-dimensional hydrofoil, *J. Fluid Mech.*, *126*, 507–520.

Eldeberky, Y., and J. Battjes (1996), Parameterization of triad interactions in wave energy models, in *Coastal Dynamics '95*, edited by W. Dally and R. Zeidler, pp. 140–148, Am. Soc. of Civ. Eng., New York.

Elgar, S., R. T. Guza, B. Raubenheimer, T. H. C. Herbers, and E. Gallagher (1997), Spectral evolution of shoaling and breaking waves on a barred beach, *J. Geophys. Res.*, *102*, 15,797–15,805.

Feddersen, E. L., S. Elgar, R. T. Guza, and T. H. C. Herbers (1998), Alongshore momentum balances in the nearshore, *J. Geophys. Res.*, *103*, 15,667–15,676.

Filipot, J.-F., F. Ardhuin, and A. V. Babanin (2010), A unified deep-to-shallow water wave-breaking probability parameterization, *J. Geophys. Res.*, *115*, C04022, doi:10.1029/2009JC005448.

Gagnaire-Renou, E. (2010), Ocean wave spectrum properties as derived from quasi-exact computations of nonlinear wave-wave interaction, *J. Geophys. Res.*, *115*, C12058, doi:10.1029/2009JC005665.

Gallagher, E. L., S. Elgar, and E. B. Thornton (1998), Megaripple migration in a natural surf zone, *Nature*, *394*(6689), 165–168.

Gelci, R., H. Cazalé, and J. Vassal (1957), Prévision de la houle. La méthode des densités spectroangulaires, *Bull. Inf. Com. Oceanogr. Etud. Cotes*, *9*, 416–435.

Hasselmann, K. (1974), On the spectral dissipation of ocean waves due to white capping, *Boundary Layer Meteorol.*, *6*, 107–127.

Hasselmann, K., R. K. Raney, W. J. Plant, W. Alpers, R. A. Shuchman, D. R. Lyzenga, C. L. Rufenach, and M. J. Tucker (1985), Theory of synthetic aperture radar ocean imaging: A MARSEN view, *J. Geophys. Res.*, *90*(C3), 4659–4686.

Hwang, L.-S., and D. Divoky (1970), Tsunami generation, *J. Geophys. Res.*, *75*(33), 6802–6817.

Janssen, P. A. E. M. (2009), On some consequences of the canonical transformation in the Hamiltonian theory of water waves, *J. Fluid Mech.*, *637*, 1–44, doi:10.1017/S0022112009008131.

Janssen, P. A. E. M., K. Hasselmann, S. Hasselmann, and G. J. Komen (1994), Parameterization of source terms and the energy balance in a growing wind sea, in *Dynamics and Modelling of Ocean Waves*, edited by G. J. Komen et al., pages 215–238, Cambridge Univ. Press, Cambridge, U. K.

Janssen, P. A. E. M., O. Saetra, C. Wettre, and H. Hersbach (2004), Impact of the sea state on the atmosphere and ocean, *Ann. Hydrogr.*, *3*(772), 3.-1–3.23.

Janssen, T. T., and J. Battjes (2007), A note on wave energy dissipation over steep beaches, *Coastal Eng.*, *54*, 711–716.

Lamb, H. (1932), *Hydrodynamics*, 6th ed., 738 pp., Cambridge Univ. Press, Cambridge, U. K.

LeMéhauté, B. (1962), On non-saturated breakers and the wave run-up, paper presented at 8th International Conference on Coastal Engineering, Am. Soc. of Civ. Eng., Mexico City.

Longuet-Higgins, M. S., and J. S. Turner (1974), An 'entraining plume' model of a spilling breaker, *J. Fluid Mech.*, *63*, 1–20.

Melville, W. K. (1994), Energy dissipation by breaking waves, *J. Phys. Oceanogr.*, *24*, 2041–2049.

Miche, A. (1944), Mouvements ondulatoires de la mer en profondeur croissante ou décroissante. Forme limite de la houle lors de son déferlement. Application aux digues maritimes. Troisième partie. Forme et propriétés des houles limites lors du déferlement. Croissance des vitesses vers la rive, *Ann. Ponts Chaussees*, *114*, 369–406.

Phillips, O. M. (1984), On the response of short ocean wave components at a fixed wavenumber to ocean current variations, *J. Phys. Oceanogr.*, *14*, 1425–1433.

Pierson, W. J., Jr., and L. Moskowitz (1964), A proposed spectral form for fully developed wind seas based on the similarity theory of S. A. Kitaigorodskii, *J. Geophys. Res.*, *69*(24), 5181–5190.

Queffeulou, P., and D. C. Fillon (2008), Global altimeters data sets, version 4, october 2008, technical report, Ifremer, Brest, France.

Rapp, R. J., and W. K. Melville (1990), Laboratory measurements of deep-water breaking waves, *Philos. Trans. R. Soc. London*, *331*, 735–800.

Rascle, N., and F. Ardhuin (2009), Drift and mixing under the ocean surface revisited. stratified conditions and model-data comparisons, *J. Geophys. Res.*, *114*, C02016, doi:10.1029/2007JC004466.

Rascle, N., F. Ardhuin, P. Queffeulou, and D. Croizé-Fillon (2008), A global wave parameter database for geophysical applications. Part 1: Wave-current-turbulence interaction parameters for the open ocean based on traditional parameterizations, *Ocean Modell.*, *25*, 154–171, doi:10.1016/j.ocemod.2008.07.006.

Ruessink, B. G., K. T. Houwman, and P. Hoekstra (1998), The systematic contribution of transporting mechanisms to the cross-shore sediment transport in water depths of 3 to 9 m, *Mar. Geol.*, *152*, 295–324.

Ruessink, B. G., D. J. R. Walstra, and H. N. Southgate (2003), Calibration and verification of a parametric wave model on barred beaches, *Coastal Eng.*, *48*, 139–149.

Saha, S., et al. (2010), The NCEP climate forecast system reanalysis, *Bull. Am. Meterol. Soc.*, *91*, 1015–1057.

Scott, N. S., E. J. Walsh, and P. A. Hwang (2005), Observations of steep wave statistics in open ocean waters, *J. Atmos. Oceanic Technol.*, *22*, 258–271.

Stansell, P., and C. MacFarlane (2002), Experimental investigation of wave breaking criteria based on wave phase speeds, *J. Phys. Oceanogr.*, *32*, 1269–1283.

Stive, M. (1984), Energy dissipation in waves breaking on gentle slopes, *Coastal Eng.*, *8*, 99–127.

Stoker, J. (1957), *Water Waves: The Mathematical Theory With Applications*, Interscience, New York.

Svendsen, I. A. (1984), Wave heights and set-up in a surf zone, *Coastal Eng.*, *8*, 303–329.

Thornton, E. B., and R. T. Guza (1983), Transformation of wave height distribution, *J. Geophys. Res.*, *88*(C10), 5925–5938.

Tolman, H. L. (2002), User manual and system documentation of WAVEWATCH-III version 2.22, *Tech. Note 222*, Natl. Oceanic and Atmos. Admin., Washington, D. C.

Tolman, H. L. (2008), A mosaic approach to wind wave modeling, *Ocean Modell.*, *25*, 35–47, doi:10.1016/j.ocemod.2008.06.005.

Tolman, H. L., M. L. Banner, and J. M. Kaihatu (2011), The NOPP operational wave improvement project, paper presented at 12th International

Workshop of Wave Hindcasting and Forecasting, Environ. Can., Kohala Coast, Hawaii, 30 Oct. to 4 Nov.

Tracy, B. A., and D. T. Resio (1982), Theory and calculation of the nonlinear energy transfer between sea waves in deep water, *Tech. Rep. 11*, U.S. Army Eng. Waterw. Exp. Stn., Vicksburg, Miss.

van der Westhuysen, A. J. (2010), Modeling of depth-induced breaking under finite depth wave growth conditions, *J. Geophys. Res.*, *115*, C01008, doi:10.1029/2009JC005433.

van Vledder, G. P. (2006), The WRT method for the computation of nonlinear four-wave interactions in discrete spectral wave models, *Coastal Eng.*, *53*, 223–242.

van Vledder, G. P., T. H. C. Herbers, R. E. Jensen, D. T. Resio, and B. Tracy (2000), Modelling of non-linear quadruplet wave-wave interactions in operational wave models, in *Coastal Engineering 2000: Conference Proceedings: July 16–21, 2000, Sydney, Australia*, edited by B. L. Edge, pp. 797–811, Am. Soc. of Civ. Eng., Reston, Va.

WAMDI Group (1988), The WAM model—A third generation ocean wave prediction model, *J. Phys. Oceanogr.*, *18*, 1775–1810.

Webb, D. J. (1978), Nonlinear transfer between sea waves, *Deep Sea Res.*, *25*, 279–298.

WISE Group (2007), Wave modelling—The state of the art, *Prog. Oceanogr.*, *75*, 603–674, doi:10.1016/j.pocean.2007.05.005.

Wu, C. H., and H. M. Nepf (2002), Breaking criteria and energy losses for three-dimensional wave breaking, *J. Geophys. Res.*, *107*(C10), 3177, doi:10.1029/2001JC001077.

Young, I. R., and L. A. Verhagen (1996), The growth of fetch-limited waves in water of finite depth. Part 1. Total energy and peak frequency, *Coastal Eng.*, *29*, 47–78.

F. Ardhuin, Laboratoire d'Océanographie Spatiale, Ifremer, Centre de Brest, B.P. 70, F-29280 Plouzané, France. (fabrice.ardhuin@ifremer.fr)

J.-F. Filipot, Service Hydrographique et Océanographique de la Marine, 14 Rue du Chatellier, F-29200 Brest, France. (filipot@shom.fr)